2026 IEEE/SICE International Symposium on System Integration (SII)
January 11-14, 2026. Cancún, México

Image Resolution Enhancement Using Time-of-Flight-Based Backscatter Rejection in Compton Camera

Yosuke Kobayashi[1], Koki Nakamura[1], Agus Nur Rachman[2], Tadashi Orita[1], Mizuki Uenomachi[3], Hideki Tomita[4], Yusuke Tamura[5], Kei Kamada[5], Fumihiko Ishida[6], Eiji Takada[6], Jun Kawarabayashi[7], Kosuke Tanabe[8], Ken'ichi Tsuchiya[8],Hanwool Woo[9], Kenji Shimazoe[1].

[1]The University of Tokyo, Tokyo, Japan, [2]National Research and Innovation Agency, Jakarta, Indonesia [3]Institute of Science Tokyo, Tokyo, Japan, [4]Nagoya University, Nagoya, Japan [5]Tohoku University, Sendai, Japan, [6]National Institute of Technology, Toyama College, Toyama, Japan, [7]Tokyo City University, Tokyo, Japan,[8]National Research Institute of Police Science, [9]Kogakuin University, Tokyo, Japan.

***Abstract*—This study presents a technique to enhance Compton camera imaging used for radioactive source localization in security applications. A key issue in Compton imaging is "backscattering events," where gamma-ray interactions are misordered—such as when the absorber records a hit before the scatterer—leading to incorrect Compton cone reconstruction and image artifacts. To address this, the research applies the Time-of-Flight (TOF) principle to determine the correct interaction sequence.**

A detector system comprising GFAG scintillators, SiPMs, and a custom ASIC/DAQ setup achieves a 296 ps coincidence time resolution, sufficient to resolve 4.4 cm-scale interaction order. TOF values are calculated per event after correcting for systematic effects, allowing identification and rejection of backscattering events. Applying this TOF-based filtering significantly improves the signal-to-noise ratio. The resulting data, processed with the MLEM algorithm, yields an angular resolution (ARM) of 13.3°–16.5° (FWHM), aligning well with Geant4 simulations. This demonstrates TOF filtering as an effective method for enhancing Compton imaging quality.

I. Introduction

Remote teleoperation of robots for disaster response, inspection, and unmanned construction requires in-situ, real-time visualization of both the environment and hazards to support operator decision-making. In radiological scenarios, rapidly localizing illicit or orphan radioactive sources is essential for safe standoff operation and task planning [1,2].

Gamma-ray imaging—particularly Compton cameras—reconstructs the origin of incident photons from multiple interactions within the detector [3,4]. Notably, 4π Compton imagers have demonstrated wide-field source localization [5]. A key limitation, however, is ambiguity in the interaction sequence: if hits are misordered, backscatter-like solutions broaden the point-spread function (PSF) and degrade localization accuracy [6].

We apply a time-of-flight (TOF) event-ordering filter that evaluates whether the measured inter-hit time is consistent with the geometric flight time between detectors within the system timing resolution. TOF discrimination, widely used in PET imaging, assumes a Gaussian timing distribution, where events within ±3σ are retained as true coincidences while outliers are rejected [7–12]. In our implementation (CTR = 296 ps FWHM; σ ≈ CTR/2.355) with 150 mm detector spacing, a ±500 ps (≈ 4σ) acceptance window was applied, preserving ≈ 99.99 % of valid events and improving image sharpness by excluding misordered interactions.

From a system-integration viewpoint, the TOF gate provides a lightweight, low-latency selection stage that can run on the acquisition path and feed list-mode MLEM reconstruction, enabling real-time overlays of radiation hot-spots on robot maps or video for teleoperation. Recent advances in compact Compton cameras have demonstrated successful real-time integration with robotic and aerial platforms, enabling 3D mapping and remote radiation monitoring [13, 14]. The approach is compatible with fast scintillator/SiPM modules (e.g., GFAG/GAGG with SiPMs) and related PET/Compton developments [15].

Building on these, this work contributes: (i) a physically motivated TOF gate (±500 ps ≈ 4σ at L = 150 mm) for event-by-event hit-order selection, and (ii) experimental evaluation showing improved angular resolution and source localization suitable for remote visualization in robotic teleoperation.

As a precedent for the development of a Compton camera for the above purpose, in 2014, Anthony Sweeney of the University of Liverpool developed a Compton camera

consisting of two semiconductor double-sided strip detectors. This system was designed to identify and locate radioactive isotopes emitting gamma rays in the energy range of 60 to 1408 keV for the purpose of domestic security [16].

II. METHODOLOGY

Gamma-ray imaging system setup

The detector at the core of the Compton camera system developed in this research consists of a series of interconnected components that work together, from gamma-ray capture to data acquisition. First, the scintillator captures gamma rays and converts them into visible light. Next, the SiPM (Silicon Photomultiplier) reads this faint visible light emitted from the scintillator, converting and amplifying it into an electrical signal. Subsequent signal processing is handled by the electronic circuit, which performs a series of operations including shaping the SiPM's signal waveform, setting threshold voltages, comparison using a comparator, and converting analog signals to digital. Finally, the processed data is collected and stored by the Data Acquisition System (DAQ). Each of these parts functions in coordination to achieve high-precision gamma-ray detection. From this point, we will introduce the specific functions and details of each part.

- GFAG Scintillator

Gadolinium fine aluminum gallate (GFAG) is the fast type of GAGG Crystal. It has short decay time, which is suitable for experimental setup where faster response is required. A 64 GFAG array is shown in Figure1.(a). The Pixel size of each GFAG is 2.5 × 2.5 × 5 mm^3. Between the crystal, Barium Sulfate (BaSO4) was used for reflector. The pitch between Crystal is 3.2 mm. The density is 6.63 g/cm^3.

Previous studies have shown that when the GFAG scintillator is paired with a Hamamatsu R6231-100 PMT, it can achieve an energy resolution of 7% (FWHM) for 662 keV gamma rays [17].

- Silicon Photomultiplier (SiPM)

A silicon photomultiplier (SiPM) is a solid-state photodetector that, in response to absorption of a photon, can produce a current pulse several tens' nanoseconds long containing 10^5 to 10^6 electrons. Figure 1.(b) presented an 8x8 channel SiPM array. At the backside of the SiPM board a micro coaxial port is mounted, which allow the SiPM to be connected to the ASIC using a micro coaxial cable (shown in Figure 1.(c)).

(a) (b) (c)

Figure 1. (a) 8 × 8 GFAG Crystal array with each crystal size 2.5 x 2.5 x 5 mm^3
(b) 64-channel MPPC array from Hamamatsu Photonic(S13361-3050)
(c) Micro Coaxial port is used to connect the MPPC for SiPM output, connected to ASIC using a Micro Coaxial cable

- Analog to Digital Processing Signal

Time over threshold (ToT) is a method converting the analog signal to digital. It converts the amplitude of the analog signal into the time width. The ToT width represents the energy information [18]. This method is embedded in the ASIC chip.

- Application-Specific Integrated Circuit (ASIC)

ASIC is a non-standard integrated circuit that has been designed for a specific use or application. ASIC may contain a very large part of the electronics [19]. The ASIC board presented in Figure 2. The ASIC have 64-channel where in each channel, it consists of a current buffer, a slew-rate limited shaper, a voltage comparator, current comparator, a monostable multivibrator, and an OR gate.

The ASIC chip has a size of 4 × 6 mm fabricated with TSMC (Taiwan Semiconductor Manufacturing Corporation) 0.25 µm CMOS process. Power consumption is 3mW.

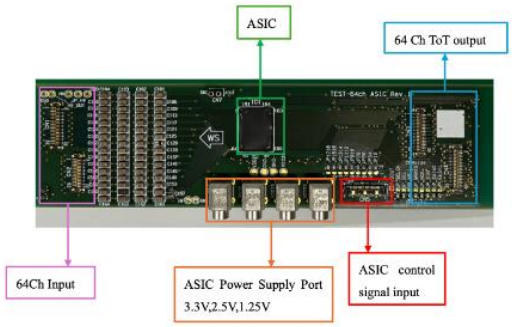

Figure 2. Setup of ASIC

- Multi-Channel High Time Resolution DAQ

Multi-channel high-time resolution Data acquisition System receiving and saving ToT signal from ASIC. The DAQ has 144 channel input and has 62.5 ps time precision. The DAQ synchronizes with time signal provide by the Time Zero (T0) board.[20]

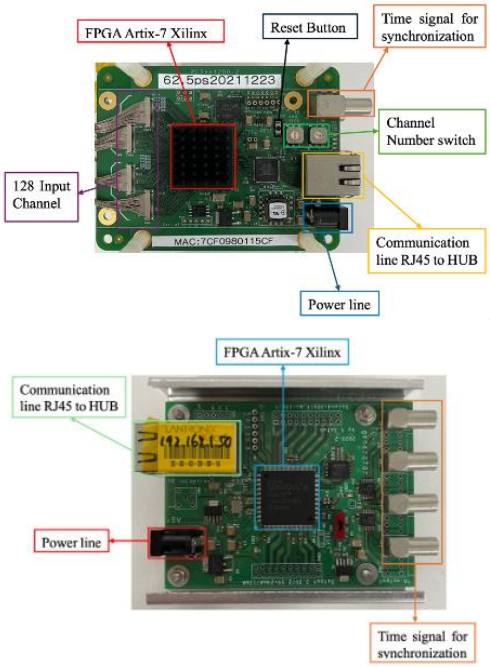

Figure 3. PETnet DAQ for ASIC data processing

Imaging reconstruction

- Simple back projection

This algorithm is the direct application of the Compton kinematics. It follows the equation below.

$$cos\theta = 1 - m_e c^2 \left(\frac{E_1}{E_0(E_0 - E_1)}\right)$$

The θ is obtained using the equation. We determine cone direction base on the axis [BA], and the projection plane is compute using information of source position from the detector as given below. E_0 is the incident photon energy, and in the Figure 4 below, E_0=E_1+E_2. E_1 is the energy absorbed in the scatter detector, and E_2 is the energy absorbed in the absorber detector.

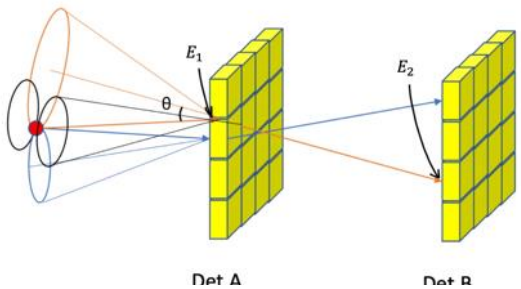

Figure 4. Diagram of Reconstruction Method

- Maximum-likelihood expectation maximization

This is an iterative method to find (local) maximum likelihood estimates of parameters in statistical models.

$$f_j^{n+1} = \frac{f_j^n}{\sum_i S_{i,j}} \sum_i \frac{S_{i,j}}{\sum_l S_{i,l} f_l^n}$$

Each of the symbols in the equation represents the following:

- f_j^n: j voxel intensity at n th iteration.
- $S_{i,j}$: System matrix, the probability that source at voxel. j is detected by LOR i
- i: list mode events
- LOR: line of response

- TOF-based Event-Ordering Filter

After channel-to-channel and time-walk corrections, the inter-hit time is defined as $\Delta t = t_2 - t_1$ .With module separation $L = 150$ mm, the expected flight times are $\pm L/c \approx \pm 500$ps.
For each hypothesis $s \in \{+1, -1\}$, the TOF residual is

$$\varepsilon_s = \Delta t - s \cdot \frac{L}{c}.$$

From the measured timing resolution CTR = 296 ps (FWHM), we set $\sigma = \mathrm{CTR}/2.355 \approx 126$ps.
The acceptance half-width is fixed a priori to

$$|\varepsilon_s| \leq 500\ ps\ (\approx 4\sigma),$$

which avoids overlap of the $\pm L/c$ windows and retains TOF-consistent events.
If either residual satisfies $|\ \varepsilon_s\ | \leq 500\ ps$, we keep the ordering with the smaller $|\ \varepsilon_s\ |$; otherwise the event is rejected.

III. Performance Evaluation and Results

Compton camera system functionalities were comprehensively evaluated, demonstrating high-precision capabilities.

A. Time Resolution Measurement

The average time resolution of our detector system was 296 ps (FWHM), allowing the distinction of arrival times for two identical events separated by 4.4 cm. Figure 5 shows the experimental setup for coincidence time resolution (CTR) measurement, using a 0.8 MBq ^{22}Na point source placed between two detectors separated by 80 mm. Figures 6 and 7 illustrate the CTR distributions before and after channel-to-channel calibration, respectively. The improvement observed in Figure 7 validates the effectiveness of the calibration in enhancing temporal precision.[21]

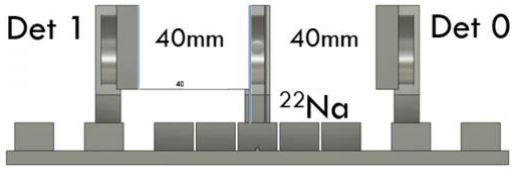

Figure 5. Time resolution measurement setup

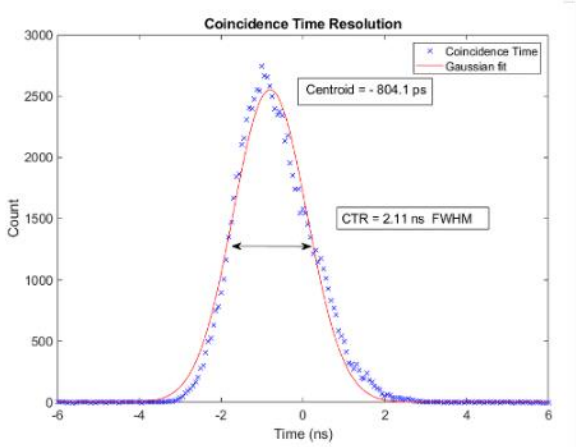

Figure 6. Coincidence time resolution measurement before channel-to-channel calibration

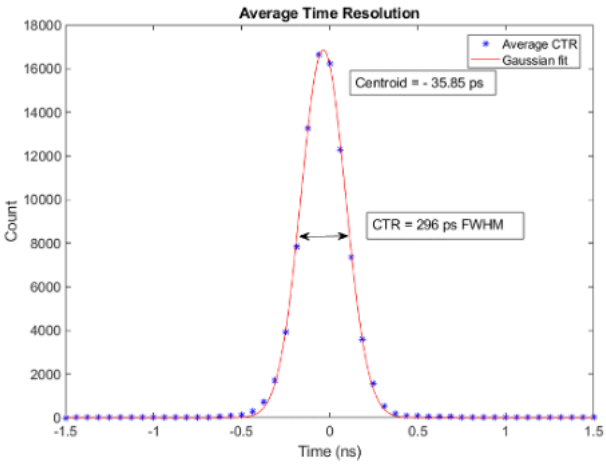

Figure 7. Coincidence time resolution measurement after channel-to-channel calibration

B. *Maintaining Energy Calibration*

Threshold levels for each ASIC channel were adjusted by monitoring the shaper and ToT output using an oscilloscope. Figure 8 presents the measured gamma-ray energy spectrum using various sources, from ^{241}Am to ^{137}Cs. The detector system achieved excellent energy resolution, with 6.54% FWHM at 511 keV and 5.21% at 662 keV. Figure 9 shows the correlation between gamma-ray energy and ToT width, highlighting the nonlinear response at higher energies due to SiPM saturation.

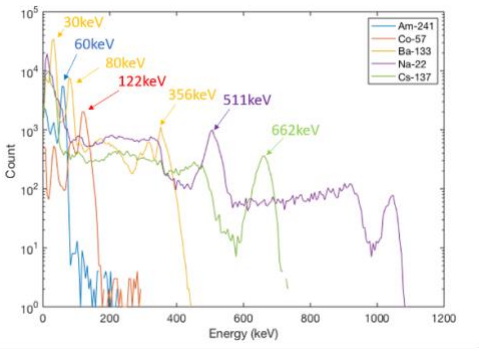

Figure 8. Energy spectrum from ^{241}Am, ^{133}Ba, ^{57}Co, ^{22}Na, and ^{137}Cs.

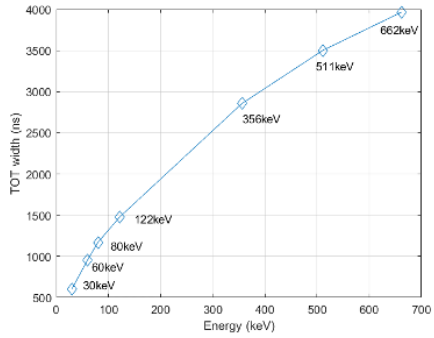

Figure 9. Linearity of the gamma-ray energy and the ToT width.

C. *Time Walk Calculation and Correction*

To accurately recover the interaction order, the energy-dependent time-walk phenomenon was quantitatively evaluated. Time-walk was calculated across an energy range of 30-490 keV, with 10 keV steps and ±5 % energy resolution.

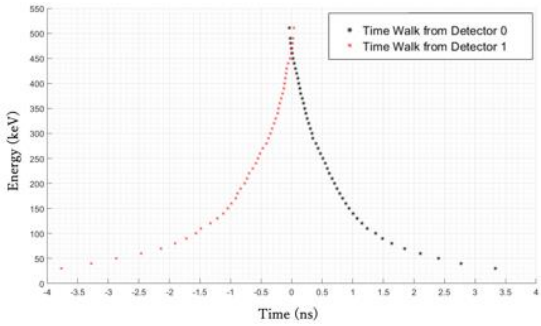

Figure 10. Time-walk calculation result from Detector 0 and 1

Figure 10 comprehensively illustrates the time-walk characteristics for both Detector 0 and Detector 1, showing the variation of time shift across different energy ranges. For Detector 0, time-walk ranged from 3.33 ns (30 keV) to <700 ps (210-490 keV). Detector 1 showed similar, slightly longer time-walks, ranging from 3.76 ns (30 keV) to <700 ps (220-490 keV). This difference is attributed to variations in individual channel sensitivity.

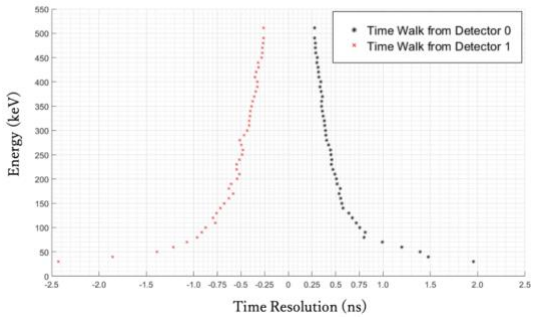

Figure 11. Time Resolution from time-walk calculation result in Detector 0 and 1

Figure 11 further details the derived time resolution from these time-walk calculations, highlighting the energy dependence of timing performance. While low-energy (30-170 keV) time-walk correction proved challenging, energies above 200 keV consistently yielded time-walks less than 900 ps and time resolutions below 500 ps, affirming the feasibility of applying time-walk correction in this range for improved accuracy.

D. Compton Imaging and ARM Enhancement

Geant4 simulations estimated an Angular Resolution Measure (ARM) of 15.78° (FWHM). Experimental measurements using a ^{137}Cs source yielded ARM values ranging from 13.3° to 16.5° (FWHM), which are consistent with the simulation results and validate the performance of the developed Compton camera system.

To further investigate the effect of time-of-flight (TOF)-based filtering, an experiment was conducted using a source position, as illustrated in Figure 12**.**

Figure 13 shows the energy maps of all Compton coincidence times in the detector. To quantify the improvement, ARM distributions were analyzed under both conditions.

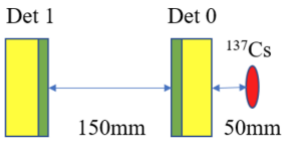

Figure 12. Compton detector experiment with a source position

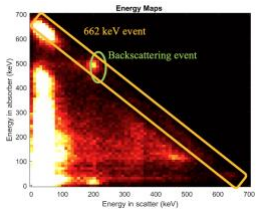

Figure 13. Compton Coincidence time for the forward scattering and backscattering from two source positions.

Figure 14 shows the time distributions of coincidence events with a scatter energy of 200 keV ± 5%. After applying channel-to-channel timing correction, forward- and backscattering events are clearly separated with a time difference of 0.84 ns, as illustrated in Figure 14 (a). Subsequently, energy-dependent time-walk correction was applied to compensate for the slower timing response of the 200 keV signal, which was paired with a 462 keV absorber event. As a result, the coincidence time peaks for forward and backscattering events shifted to –0.41 ns and +0.44 ns, respectively, as shown in Figure 14 (b). These values closely match the expected ±0.5 ns separation, confirming that the time-walk correction successfully recovers the correct interaction order and contributes to improving the fidelity of image reconstruction.

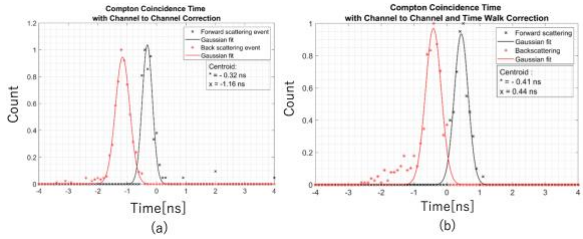

Figure 14. Compton Coincidence time for the forward scattering and backscattering from coincidence time which scatter energy is 200 keV ± 5 %, (a) before channel-to-channel and time-walk correction, (b) after channel-to-channel and time-walk correction

Figure 15 shows the reconstructed images using the MLEM algorithm with five iterations. Figure 15 (a) includes all coincidence events, while panel Figure 15 (b) includes only forward-scattering events selected by TOF-based filtering. The filtered image demonstrates improved source localization and reduced background artifacts.

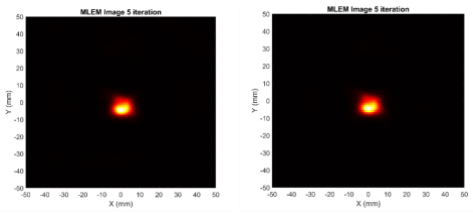

(a) (b)

Figure 15. Compton imaging using MLEM 5 iteration.

(a). The image reconstruction from the coincidence time with unsorted 200 keV data

(b). The image reconstruction from the coincidence time with forward scattering in the 200 keV data.

Figure 16 shows the angular resolution distributions (ARM) obtained from both unfiltered and filtered datasets. The ARM improved from 16.65° to 14.98° FWHM after applying TOF-based event selection, corresponding to a ~10% enhancement in angular resolution.

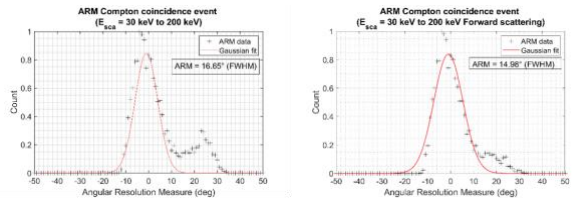

(a) (b)

Figure 16.

(a): ARM for the from the coincidence time with unsorted 200 keV data

(b): ARM for the from the coincidence time with forward scattering. event in 200 keV data

IV. Conclusion And Future Work

This study reports on an endeavor to apply the Time-of-Flight (TOF) principle to a Compton camera system, aiming to enhance its imaging performance for accurate radioactive source localization and time walk and time resolution depending on the deposited energy are quantified in GFAG-SiPM system with ASIC. A particular focus was placed on mitigating image artifacts caused by "backscattering events," which arise from the misidentification of gamma-ray interaction sequences.

Key findings from this research include that the developed detector system achieved an average time resolution of 296 ps (FWHM) in a two-detector setup. This suggests the capability to distinguish arrival times of identical events separated by as little as 4.4 cm. The implementation of channel-to-channel and energy-dependent time-walk corrections was a notable contribution. These corrections allowed for effective compensation of detector-specific timing variations and nonlinear energy responses. Consequently, a clear temporal separation of forward-scattering and backscattering events was observed, which aided in recovering the correct interaction order within the Compton detector system. The practical impact of TOF-based filtering on Compton imaging was evaluated. By selectively including only forward-scattering events for image reconstruction, an approximate 10% enhancement in Angular Resolution Measure (ARM) was observed, improving it to 14.98° (FWHM) from 16.65° (FWHM) for unfiltered data. This is believed to contribute to a reduction in image artifacts and an increase in the fidelity of source localization.

The results obtained in this study suggest that applying TOF principles to Compton camera systems is a viable approach for improving the resolution and fidelity of gamma-ray imaging. Looking ahead, a significant area for future research involves further enhancing the system's time resolution, particularly for low-energy gamma rays. Improved timing performance in this range is expected to broaden the applicability of the TOF filtering method to a wider variety of radioactive isotopes and scenarios.

References

[1] Ajlouni, A. W., Alnairi, M. M., Albarkaty, K. S., & Alsufyani, S. J. (2023). Nuclear security in public events. *Journal of Radiation Research and Applied Sciences*, *16*(2), 100572.

[2] Barnett, D. J., Parker, C. L., Blodgett, D. W., Wierzba, R. K., & Links, J. M. (2006). Understanding radiologic and nuclear terrorism as public health threats: preparedness and response perspectives. *Journal of Nuclear Medicine*, *47*(10), 1653-1661.

[3] Orita, T., Yabu, G., Yoneda, H., Takeda, S. I., Caradonna, P., Takahashi, T., ... & Shimazoe, K. (2021). Double-photon emission imaging with high-resolution Si/CdTe Compton cameras. *IEEE Transactions on Nuclear Science*, *68*(8), 2279-2285.

[4] Roser, J., Hueso-González, F., Ros, A., & Llosá, G. (2021). Compton cameras and their applications. In *Radiation detection systems* (pp. 161-198). CRC Press.

[5] Tomita, Hideki, et al. "Gamma-ray source identification by a vehicle-mounted 4π Compton imager." *2020 IEEE/SICE International Symposium on System Integration (SII)*. IEEE, 2020.

[6] Calderón, Y., Chmeissani, M., Kolstein, M., & De Lorenzo, G. (2014). Evaluation of Compton gamma camera prototype based on pixelated CdTe detectors. *Journal of Instrumentation*, *9*(06), C06003.

[7] Zhihong, Z., Shimazoe, K., & Takahashi, H. (2022). Characterization of time-of-flight double-photon Compton imaging system by simulation. *Journal of Instrumentation*, *17*(01), C01045.

[8] Wen, J., Zheng, X., Gao, H., Zeng, M., Zhang, Y., Yu, M., ... & Zhao, Z. (2022). Optimization of Timepix3-based conventional Compton camera using electron track algorithm. *Nuclear Instruments and Methods in Physics Research Section A: Accelerators, Spectrometers, Detectors and Associated Equipment*, *1021*, 165954.

[9] T. F. Budinger, "Time-of-flight positron emission tomography: status relative to conventional PET," J. Nucl. Med., vol. 24, pp. 73–78, 1983.

[10] S. Surti and J. S. Karp, "Investigation of time-of-flight benefit for fully 3D PET," IEEE Trans. Med. Imaging, vol. 25, no. 5, pp. 529–538, 2006.

[11] V. C. Spanoudaki and C. S. Levin, "Photo-Detectors for Time-of-Flight Positron Emission Tomography (TOF-PET)," Sensors, vol. 10, no. 12, pp. 10484–10505, 2010.

[12] M. Conti and B. Bendriem, "The new opportunities for high time resolution clinical TOF PET," Clin. Transl. Imaging, vol. 7, pp. 139–147, 2019.

[13] S. Kim and J. S. Lee, "Development and Applications of Compton Camera — A Review," Sensors, vol. 22, no. 7374, pp. 1–25, 2022.

[14] M. Werner et al., "Autonomous Localization of Multiple Ionizing Radiation Sources Using Miniature Single-Layer Compton Cameras Onboard a Group of Micro Aerial Vehicles," in Proc. IEEE/RSJ Int. Conf. Intell. Robots Syst. (IROS), Abu Dhabi, UAE, Oct. 2024.

[15] Kim, S. M., & Lee, J. S. (2024). A comprehensive review on Compton camera image reconstruction: from principles to AI innovations. *Biomedical Engineering Letters*, *14*(6), 1175-1193.

[16] A. Sweeney, "Compton Imaging for Homeland Security by," no. April, 2014

[17] Iwanowska-Hanke, J., Brylew, K., Witkowski, M. E., Sibczynski, P., Szczesniak, T., Moszynski, M., ... & Kamada, K. (2020). Cerium-doped gadolinium fine aluminum gallate in scintillation spectrometry. *Nuclear Instruments and Methods in Physics Research Section A: Accelerators, Spectrometers, Detectors and Associated Equipment*, *979*, 164464.

[18] Shimazoe, K., Takahashi, H., Omura, T., Orita, T., & Yamashita, T. (2012). Dynamic time-over-threshold method for pulse shape discrimination. *IEEE Transactions on Nuclear Science*, **59**(6), 3213–3217.

[19] Orita, T., Uenomachi, M., Shimazoe, K., & Ikeda, H. (2023). Time and energy resolving time-over-threshold ASIC for MPPC module in TOF-PET system (ToT-ASIC2). *Journal of Instrumentation*, **18**(09), P09033.

[20] Sato, S., Uenomachi, M., Shimazoe, K.,(2021). Development of multichannel high time resolution data acquisition system for TOT-ASIC. *IEEE Transactions on Nuclear Science* 68.8: 1801-1806.